RSC Advances

ROYAL SOCIETY OF CHEMISTRY

www.rsc.org/advances

RSC Advances

PAPER

Uncapped Au-Pd colloidal nanoparticles show catalysis enhancement

Received 00th January 20xx,
Accepted 00th January 20xx

DOI: 10.1039/x0xx00000x

www.rsc.org/

Min-Tsang Li,[a,b] Chang-Hai Wang,[a] Sheng-Feng Lai,[a] Yu-Han Chen,[a] Edwin B. L. Ong,[a] Chung-Kwei Lin,[c,d] G. Margaritondo[e] and Y. Hwu*[a,b,f]

The catalytic properties of Pd trigger a strong interest on the related catalysis by Au-Pd nanoparticles. However, the analysis of such phenomena was complicated so far by the presence of capping. Using x-ray irradiation, we could produce uncapped Au-Pd nanoparticles and study their catalytic features, finding in particular their relation to the Pd content. Furthermore, the fabrication process is *per se* interesting, yielding excellent and flexibly controllable nanoparticles with a rather simple procedure.

1. Introduction

X-ray irradiation, an approach that was widely and positively tested on other nanosystems, yielded in our study excellent Au-Pd nanoparticles with a simple process. The products and in particular their composition-dependent structural and optical properties were extensively characterized by X-ray diffraction (XRD), UV-VIS (ultraviolet-visible) optical spectroscopy, X-ray absorption near edge spectroscopy (XANES) and transmission electron microscopy (TEM). We could control the structure and particle size by acting on the precursor solution composition, changing from alloyed Au-Pd to a mixture of Au-Pd alloys and Pd. TEM revealed Pd surface segregation in the alloyed Au-Pd nanoparticles.

The most interesting implication of these results is the possibility to produce uncapped Au-Pd nanoparticles and study their catalytic properties. This yields essential information to understand catalysis by Au-Pd nanosystems, whose analysis was so far complicated by capping.

Our study is in the mainstream of the expanding interest in the catalytic applications of bimetallic nanoparticles, linked to the composition tunability, possible cost reduction and superior catalytic performance compared to their monometallic counterparts.[1-3] Au-Pd is one of the most important systems and the corresponding nanoparticles possess good catalytic properties for a variety of chemical reactions such as CO oxidation and hydrocarbon hydrogenation.[4-6]

So far, Au-Pd nanoparticles were mainly prepared by chemical approaches such as reduction[7-12] and the polyol process.[13, 14] Irradiation-based approaches were also used, based on X-rays,[15] electron beams,[16] gamma-rays,[17, 18] ultrasounds[19, 20] or microwaves.[21]

Capping agents play an important role in the synthesis of bimetallic nanoparticles, guaranteeing for example stability. The price to pay in catalytic studies is that capping complicates the issues by influencing the catalytic properties. Capping may in fact negatively affect or even suppress the reactivity[15] and may require burning it out to recover the catalytic function. It would be thus desirable to analyze bimetallic nanoparticle catalysis without capping: this is what we accomplished with our approach. Alternate methods to produce uncapped nanoparticles, such as vapor or molecular beam deposition[22] are not immune from problems, in particular as far as size and composition control is concerned. Here, we used a combined physico-chemical approach based on intense –ray irradiation that removes such problems. The success of this approach depends on the powerful reducing capacity of intense X-rays from a synchrotron radiation source; in other context, it did produce excellent Au-Pt nanoparticle.[15] In synthesis, our Au-Pd nanoparticles are not only excellent and with good catalytic properties, but also flexibly controllable by changing the process parameters.

2. Experimental

2.1 Materials and Methods

[a] *Institute of Physics, Academia Sinica, Taipei 11529, Taiwan*
[b] *Department of Engineering Science, National Cheng Kung University, Tainan 70100, Taiwan*
[c] *Department of Material Science and Engineering, Feng-Jia University, Taichung 407, Taiwan*
[d] *School of Dental Technology, College of Oral Medicine, Taipei Medical University, Taipei 11031, Taiwan*
[e] *Faculté des scences de base, Ecole Polytechnique Fédérale de Lausanne (EPFL), CH-1015 Lausanne, Switzerland*
[f] *Advanced Optoelectronic Technology Center, National Cheng Kung University, Tainan 70100, Taiwan.*
† *Corresponding author: E-mail: phhwu@sinica.edu.tw.

All commercial-grade chemicals were used as received. The aqueous precursor solution contained $HAuCl_4 \cdot 3H_2O$ (10 mM, Aldrich, MO, US) and $PdCl_2$ (10 mM, Seedchem company PTY. LTD, Melbourne, Australia). $PdCl_2$ powders were not completely soluble in de-ionized water, thus were first dissolved in concentrated hydrochloride acid. The desired $PdCl_2$ concentration was achieved by adding de-ionized (DI) water. A co-reduction approach was adopted and the precursor Au^{3+}_x/Pd^{2+}_{1-x} composition was in the range x = 0-1.0). The total metal concentration was 1 mM. In a typical fabrication process, 10 ml of the precursor solutions containing 0.5 mM Au^{3+} and 0.5 mM Pd^{2+} were put in a 15 ml polypropylene conical tube. Exposure to X-rays followed for 5 min at the BL01A beamline of the National Synchrotron Radiation Research Center (NSRRC, Hsinchu, Taiwan).[23,24] Monometallic Au and Pd nanoparticles were prepared under identical conditions for comparison.

In an alternate (small-volume) approach, 0.7 ml of pre-mixed precursor solutions with 1 mM metal concentration was put in a 1 ml PS cuvette. The cross-section of the precursor solution was completely covered by the incident X-ray beam and the exposure time was 12 sec to guarantee the complete reduction of the metallic ions.

2.2 Materials and Methods

Synchrotron powder XRD measurements were performed on the NSRRC beamline BL13A (wavelength = 0.1027 nm). To collect a sufficient amount of nanoparticles, the Au-Pd colloidal solutions were condensed with an Eppendorf 5810R high speed centrifuge and with Amicon Ultra-15, Millipore centrifugal filters, at 3200 g for 30 min. Drying at 45 °C under atmospheric conditions followed.

Transmission XANES measurements at Au L_3 edge were performed at the NSRRC 01C1 and 17C1 beamlines. The particle size, morphology, and composition were analyzed by a JEOL JEM-2100F TEM operating at 200 kV and by energy dispersive x-ray spectroscopy (EDS). For TEM sample preparation, solution drops were put on carbon coated copper grids and let to dry. The average particle size was evaluated from the images by inspecting >100 individual particles.

The key part of our study was the analysis of catalytic performances. This was done by studying the reduction of *p*-nitrophenol (PNTP) to *p*-aminophenol in the presence of $NaBH_4$. All aqueous solutions were freshly prepared right before their use. A typical test was performed by mixing 1 ml 0.2 mM *p*-nitrophenol, 0.7 ml DI water and 0.2 ml 0.1M $NaBH_4$ in a quartz cuvette. The color of solution turned light yellow right after adding the borohydride. The reaction started after adding 0.1 ml of the 0.1mM nanoparticle solution ; the bleaching of the *p*-nitrophenol solution, as detected by the absorbance decrease at 400 nm, was monitored by a UV-VIS USB4000 Ocean Optics spectrophotometer.

3. Results and discussion

3.1 Formation of Au-Pd alloyed nanoparticles by optical absorption spectroscopy

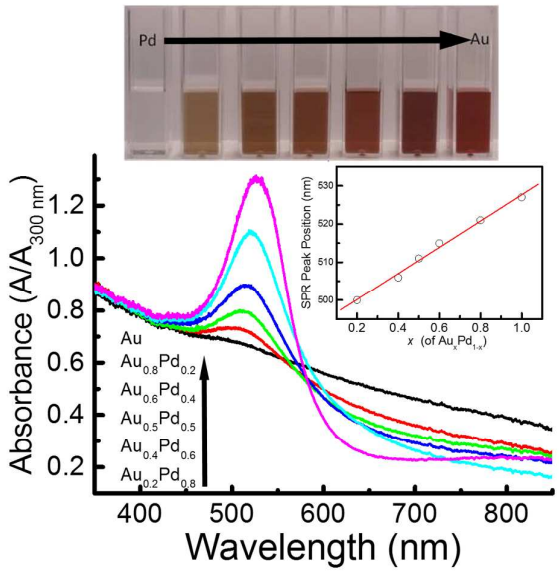

Fig. 1 UV-VIS optical absorption spectra of bimetallic Au-Pd nanoparticles for different Au/Pd values (x). The inset shows plots the SPR peak intensity vs x, with a linear best fit. The visual appearance of the Au-Pd nanoparticle solution is shown in the photograph for x = 0, 0.2, 0.4, 0.5, 0.6, 0.8, 1.0.

Figure 1 shows the UV-VIS absorption spectra of Au-Pd nanoparticles for different Au/Pd ratios. The surface plasmon resonance (SPR) peak consistently shifts to longer wavelength - eventually reaching the value for gold colloids - as the ratio increases and the strength increases. The inset plot shows a linear relation between the wavelength of the SPR peak and the Au/Pd ratio. This is consistent with the simulation results[19] based on the Mie theory. This indicates that our nanoparticles are a Au-Pd alloy.

As shown by the picture in Fig. 1, the Au-Pd nanoparticle colloid changes colors as the Au/Pd ratio increases -- from light brown to red. Pure Pd colloidals are opaque with a dark brown color after irradiation and precipitate in a short time.

To exclude the possibility of the formation of a mixture of Pd and Au nanoparticles, monometallic Au and Pd nanoparticles were separately synthesized and then mixed to achieve the same Au/Pd ratios as in Figure 1. The SPR absorption peak did not shift and only its intensity increased as the ratio increased. Therefore, our Au-Pd nanoparticles are bimetallic rather than a mixture of monometallic nanoparticles.

Previous irradiation synthesis studies of Au-Pd bimetallic nanoparticles revealed a dose rate effect for precursor solutions containing capping polymers.[17] A low dose rate (~ 6 kGy hr^{-1}) and γ-ray irradiation favored the formation of Au(core)–Pd(shell) nanoparticles, whereas alloyed nanoparticles were obtained at a high dose rate (2.2 kGy sec^{-1}) with electron beam bombardment.[17] These facts are consistent with our formation of alloyed nanoparticles with high-dose-rate X-ray irradiation (11.5 kGy sec^{-1}).

3.2 Nanoparticle structure

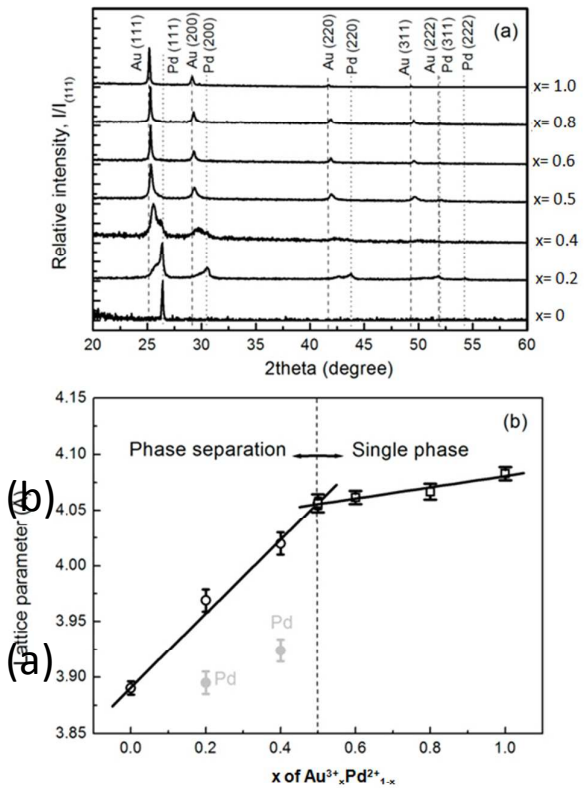

Fig. 2 Synchrotron powder XRD patterns (a) and (b) the relation of the derived lattice constant and x, with linear fits. X-ray wavelength: 1.0271 Å. Circles: data. Solid lines: linear fits.

As shown in Fig. 2(a), the XRD patterns depend on the Au/Pd ratio with the major reflections located between those of monometallic Au and Pd (111). The lattice parameters calculated from the most prominent (111) reflections are summarized in Figure 2 (b). For bimetallic nanoparticles with Au/Pd ratios x ≥ 0.5, single intense Bragg peaks were detected, which shifted to higher diffraction angles with decreasing x.

The Au-Pd system is miscible in the full composition range and generally follows the Vegard law.[25, 26] We found Au-Pd alloys to form at x ≥ 0.5. For lower x-values, separated or overlapping reflections were found between those of Au and Pd (111) – indicating phase separation. Still, the reflection shifts with x indicate partial alloying, probably coexisting with monometallic Pd nanoparticles.

Table 1 Calculated lattice constant, grain size and phase structure of Au-Pd bimetallic nanoparticles

Sample ID	Au fraction (x) in Au^{3+}_x/Pd^{2+}_{1-x}	a (Å)	Size (nm)	Phase structure
Au	1	4.083	35.6±2	Au
$Au_{0.8}Pd_{0.2}$	0.8	4.067	31.2±8	Au-Pd alloy
$Au_{0.6}Pd_{0.4}$	0.6	4.062	30.7±1	Au-Pd alloy
$Au_{0.5}Pd_{0.5}$	0.5	4.056	17.8± 5	Au-Pd alloy
$Au_{0.4}Pd_{0.6}$	0.4	4.020	9.6±2	Au-Pd alloy
		3.924	9.8±3	Au-Pd alloy
$Au_{0.2}Pd_{0.8}$	0.2	3.969	7.8±4	Au-Pd alloy
		3.895	16.6±7	Pd (?)
Pd	0	3.891	44.6±9	Pd

The effects of the precursor composition on the lattice parameter, crystal size, and phase structure are summarized in Table 1. The particle size was calculated with the Sherrer equation[27] from the (111) reflections. The particle size depends on the Au/Pd ratio: for x ≥ 0.5, Au-Pd alloyed particles are smaller than Au nanoparticles (35.6 nm) and the size decreases from 31.2 nm to 17.8 nm as x decreases. At x < 0.5, we have the smallest Au-Pd nanoparticles, 8-10 nm. The monometallic Pd nanoparticles obtained for low x-values are smaller (10-17 nm) than those for x = 0 (44.6 nm).

3.3 XANES

Figure 3 shows XANES curves for different x-values together with that of Au foil. The intensity of the L_3 spectrum is related to the number of holes in the empty d-band. The Au-Pd nanoparticles give a more intense spectrum than Au foils. Thus, the electronic properties of gold are altered by Pd, most likely due to the strong interaction of the Pd 4d band with the Au 5d band resulting in decrease of the empty density to states in the latter.

3.4 Transmission electron microscopy

As shown in Fig. 4(a), the small Au-Pd nanoparticles (x = 0.5)

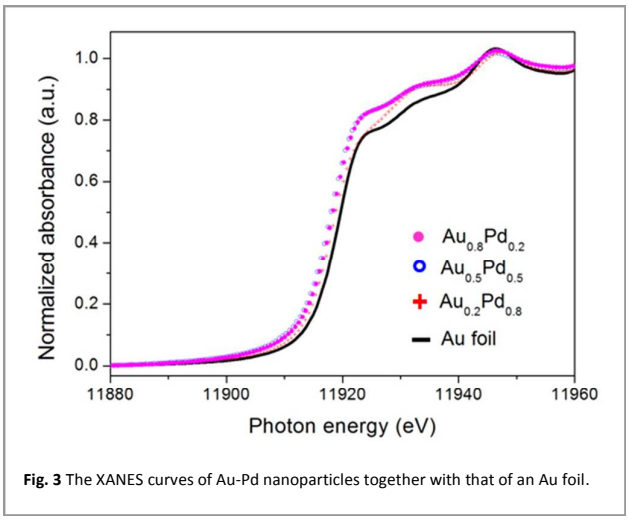

Fig. 3 The XANES curves of Au-Pd nanoparticles together with that of an Au foil.

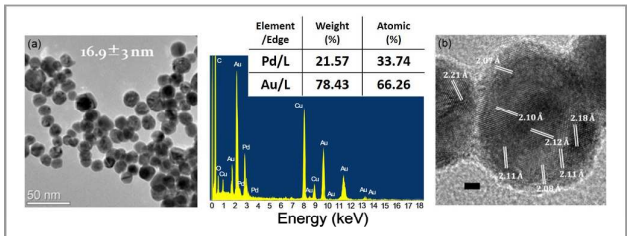

Fig. 4 TEM micrograph (a), EDS data (b) and high-resolution TEM micrograph (c) of Au-Pd (x = 0.5) bimetallic nanoparticles. Scale bar in (c): 2 nm.

are spherical and with 16.9 ± 3 nm diameter. This is consistent with the size (17.8 ± 5 nm) derived by XRD, which reflects the overall grain size for both small and aggregated nanoparticles. The EDS-derived composition, however, deviated from that of the precursor composition -- see Fig. 4(b)). Compared to microstructure-sensitive TEM and EDS, optical absorption and XRD reflect indeed the bulk nanoparticle features and are more reliable in deriving the crystal structure and the phases.

A typical high-resolution TEM micrograph of an alloyed Au-Pd nanoparticle (x = 0.5) is shown in Fig. 4(c). A core-shell-like structure is observed and the observed lattice fringes are close to the Pd {111} and {100} planes of Au-Pd alloys. For x = 0.5, the calculated d-spacing is 2.25 Å for Pd{111} planes and 2.03 Å for {100} planes. The inner part of the particle shown in the TEM picture, revealing a high electron density, could be identified with a high Au concentration. Thus, the core of the nanoparticle could be alloyed but the surface could mostly consist of segregated Pd.[20, 28-30]

3.4 Catalytic properties

The reduction of *p*-nitrophenol in the presence of $NaBH_4$ is well documented.[31-33] *p*-nitrophenol exhibits an SPR peak at 317 nm due to the formation of *p*-nitrophenolate under alkaline conditions -- that shifts to 400 nm when $NaBH_4$ is present. The solution is stable if no catalyst is added. When the reaction takes place, the 400 nm SPR peak intensity decrease and a new peak appears at 300 nm due to the formation of *p*-aminophenol. We added $NaBH_4$ to guarantee the stability of *p*-nitrophenolate; the reaction producing *p*-aminophenol can be treated as pseudo-first-order. To model its kinetics, the concentration ratio was replaced by the ratio of the SPR peak intensities A_t/A_0 measured at the times *t* and at the start of the reaction. Therefore, the reaction kinetics equation is:

$$ln\frac{c_t}{c_0} = ln\frac{A_t}{A_0} = -kT$$

where *k* is the rate constant (sec^{-1}). Figure 5 shows the plot of $ln(A_t/A_0)$ vs time for different x-values. The Au-Pd nanoparticles for the lowest x-value, 0.2, exhibit the strongest catalytic performance. The reaction was basically completed in 2 min. On the contrary, the highest x-value, 0.8, corresponds to the slowest reaction. Note that the particle size also decreases with x, suggesting a role in the enhanced catalytic properties in addition to that of the Pd content.

We did not observe the "synergistic effect" in the catalytic properties of Au-Pd nanoparticles as previously reported.[34] Note that the catalytic properties of pure Pd nanoparticles are not presented because they are not a stable colloid. However, we can argue from the trend of increasing catalytic performance with Pd concentration that such an effect is not affected by the amount of Au. It is likely that the synergistic effect is linked to capping, validating our argument that studies of uncapped nanoparticle are required to fully clarify the phenomena.

The ultrahigh flux of synchrotron X-rays can be exploited for very fast fabrication of Au-Pd nanoparticles with the already mentioned small-volume approach. Our preliminary results indicate that the uncapped Au-Pd nanoparticles so prepared with a very short exposure time (up to 12 sec) have a similar composition-dependent catalytic performance as that described above.

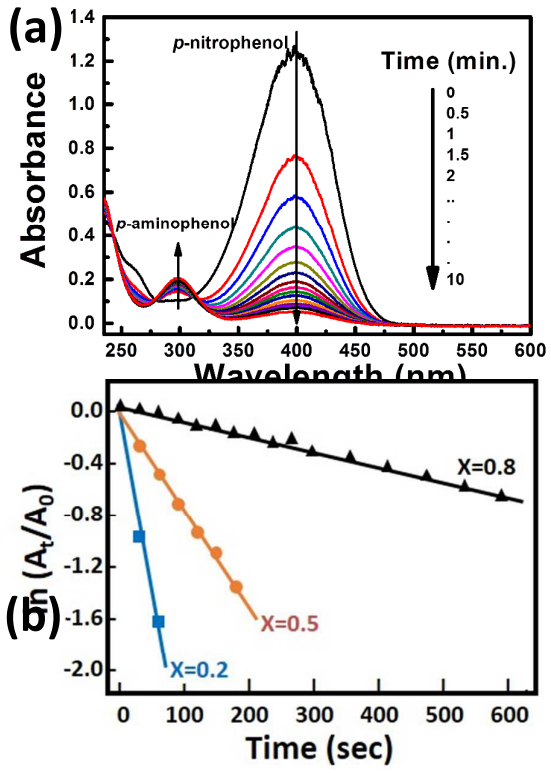

Fig. 5 The evolution of the UV-VIS absorption spectrum of *p*-nitrophenol reduced by Au-Pd bimetallic nanoparticles (a), and the plot of $ln(A_t/A_0)$ on the reaction time. for three different x-values.

Acknowledgements

This work is supported by the National Science and Technology Program for Nanoscience and Nanotechnology, the Thematic Research Project of Academia Sinica, the Biomedical Nano-Imaging Core Facility at National Synchrotron Radiation Research Center (Taiwan), the Center for Biomedical Imaging (CIBM) in Lausanne and by the EPFL.

Notes and references

1 D. Mott, J. Luo, P. N. Njoki, Y. Lin, L. Wang and C-J. Zhong, *Catal. Today*, 2007, **122**, 378.
2 D. Xu, Z. P. Liu, H. Z. Yang, Q. S. Liu, J. Zhang, J. Y. Fang, S. Z. Zou and K. Sun, *Angew. Chem. Int. Ed.*, 2009, **48**, 4217.
3 D. S. Wang and Y. D. Li, *Adv. Mater.*, 2011, **23**, 1044.
4 M. S. Chen, D. Kumar, C. W. Yi and D. W. Goodman, *Science*, 2005, **310**, 291.
5 D. Wang, A. Villa, F. Porta, D. S. Su and L. Prati, *Chem. Commun.*, 2006, 1956.
6 H. Heinz, B. L. Farmer, R. B. Pandey, J. M. Slocik, S. S. Patnaik, R. Pachter and R. R. Naik, *J. Am. Chem. Soc.*, 2009, **131**, 9704.

7 Z. B. Ge, D. G. Cahill and P. V. Braun, *J. Phys. Chem. B*, 2004, **108**, 18870.
8 M. R. Knecht, M. G. Weir, A. I. Frenkel and R. M. Crooks, *Chem. Mater.*, 2008, **20**, 1019.
9 S. Marx and A. Baiker, *J. Phys. Chem. C*, 2009, **113**, 6191.
10 Y. W. Lee, M. Kim, Z. H. Kim and S. W. Han, *J. Am. Chem. Soc.*, 2009, **131**, 17036.
11 B. Lim, H. Kobayashi, T. Yu, J. G. Wang, M. J. Kim, Z. Y. Li, M. Rycenga and Y. Xia, *J. Am. Chem. Soc.*, 2010, **132**, 2506.
12 F. Krumeich, S. Marx, A. Baikere and R. Nesper, *Z. Anorg. Allg. Chem.*, 2011, **637**, 875.
13 N. Toshima, M. Harada, Y. Yamazaki and K. Askura, *J. Phys. Chem.*, 1992, **96**, 9927.
14 D. Ferrer, A. Torres-Castro, X. Gao, S. Sepúlveda-Guzmán, U. Ortiz-Méndez and M. José-Yacamén, *Nano. Lett.*, 2007, **7**, 1701.
15 C. L. Wang, B. J. Hsao, S. F. Lai, W. C. Chen, H. H. Chen, Y. Y. Chen, C. C. Chien C C, X. Q. Cai, I. M. Kempson, Y. Hwu and G. Margaritondo, *Nanotechnology*, 2011, **22**, 065605.
16 Y. Ohkubo, M. Shibata, S. Kageyama, S. Seino, T. Nakagawa, J. Kugai, H. Nitani and T. A. Yamamoto, *J Mater Sci.*, 2012, **9**, 2142.
17 H. Remita, A. Etcheberry and J. Belloni, *J. Phys. Chem. B*, 2003, **107**, 31.
18 F. Ksar, L. Ramos, B. Keita, L. Nadjo, P. Beaunier and H. Remita, *Chem. Mater.*, 2009, **21**, 3677.
19 T. Nakagawa, H. Nitani, S. Tanabe, K. Okitsu, S. Seino, Y. Mizukoshi and T. A. Yamamoto, *Ultrason. Sonochem.*, 2005, **12**, 249.
20 C. X. Kan, W. P. Cai, C. C. Li, L. D. Zhang and H. Hofmeister, *J. Phys. D: Appl. Phys.*, 2003, **36**, 1609.
21 O. V. Belousov, N. V. Belousova, A. V. Sirotina, L. A. Solovyov, A. M. Zhyzhaev, S. M. Zharkov and Y. L. Mikhlin, *Langmuir*, 2011, **27**, 11697.
22 C. Binns, *Surf. Sci. Rep.*, 2001, **44**, 1.
23 C. J. Liu, C. H. Wang, C. L. Wang, Y. Hwu, C. Y. Lin and G. Margaritondo, *J. Synchrotron Radiat.*, 2009, **16**, 395.
24 C. H. Wang, C. C. Chien, Y. L. Yu, C. J. Liu, C. F. Lee, C. H. Chen, Y. Hwu, C. S. Yang, J. H. Je and G. Margaritondo, *J. Synchrotron Radiat.*, 2007, **14**, 477.
25 A. R. Denton A and N. W. Ashcroft, *Phys. Rev. A*, 1991, **43**, 3161.
26 A. Maeland and T. B. Flanaga, *Can. J. Phys.*, 1964, **42**, 2364.
27 H. Christopher, in "The basics of crystallography and diffraction" (Oxford University Press, New York 1997, Chap.9, pp.145-148.
28 J. K. Edwards, A. F. Carley, A. A. Herzing, C. J. Kiely and G. J. Hutchings, *Faraday Discuss.*, 2008, **138**, 225.
29 A. A. Herzing, M. Watanabe, J. K. Edwards, M. Gonte, Z. R. Tang and G. J. Hutchings, *Faraday Discuss.*, 2008, **138**, 337.
30 F. Krumeich, S. Marx, A. Baikere and R. Nesper, *Z. Anorg. Allg. Chem.*, 2011, **637**, 875.
31 J. He, W. Ji, L. Yao, Y. Wang, B. Khezri, R. D. Webster and H. Chen, *Adv. Mater.*, 2014, **26**, 4151.
32 H. Yazid, R. Adnan, M. A. Farrukh and S. A. Hamid, *J. Chin. Chem. Soc.*, 2011, **58**, 593.
33 S. K. Ghosh, M. Mandal, S. Kundu, S. Nath and T. Pal, *Applied Catalysis A: General*, 2004, **268**, 61.
34 L. Prati, A. Villa, F. Porta, D. Wang and D. Su, *Catal. Today*, 2007, **122**, 386.